

Investigation of the stability of Hopfions in the two-component Ginzburg-Landau model

Juha Jäykkä* and Jarmo Hietarinta†

Department of Physics, University of Turku, FI-20014 Turku, Finland

Petri Salo‡

*Laboratory of Physics, Helsinki University of Technology,
P.O. Box 1100, FI-02015 TKK, Espoo, Finland*

(Dated: May 4, 2019)

We study the stability of Hopfions embedded in the Ginzburg-Landau (GL) model of two oppositely charged components. It has been shown by Babaev *et al.* [Phys. Rev. B **65**, 100512 (2002)] that this model contains the Faddeev-Skyrme (FS) model, which is known to have topologically stable configurations with a given Hopf charge, the so-called Hopfions. Hopfions are typically formed from a unit-vector field that points to a fixed direction at spatial infinity and locally forms a knot with a soft core. The GL model, however, contains extra fields beyond the unit-vector field of FS model and this can in principle change the fate of topologically non-trivial configurations. We investigate the stability of Hopfions in the two-component GL model both analytically (scaling) and numerically (first order dissipative dynamics). A number of initial states with different Hopf charges are studied; we also consider a singular potential. In all the cases studied, we find that the Hopfions are unstable against scaling, mainly due to leakage of topological charge into the electromagnetic field.

PACS numbers: 74.20.De, 47.32.cd

I. INTRODUCTION

Topologically stable knots and other vortex-like structures have recently received wide interest within condensed matter physics. One reason for this is the continuous development of experimental techniques which now allow the production of vortices in various types of media. These include, e.g., Bose-Einstein condensates^{1,2}, superconductors^{3,4,5}, superfluid ³He^{6,7} and nematic liquid crystals⁸. At the same time the increased capacity of supercomputers has made it possible to study these structures numerically. Thus, in the last decade there have been many numerical studies devoted to finding stable topologically non-trivial configurations in different physical systems, including, e.g., topological unknots, knots and vortices in the Faddeev-Skyrme (FS) model^{9,10,11,12,13,14,15}, vortices in Bose-Einstein condensates^{16,17,18}, vortex atom lasers in a two-flavor Bose condensate¹⁹ and vortices in superconductors^{20,21}, liquid helium^{22,23}, liquid metallic hydrogen²⁴ and possibly even in neutron stars²⁵.

There are various ways in which a vector field in material can support vortices. For example the velocity field can form a vortex, e.g., in a hurricane. The position of the vortex is in the eye of the hurricane, where the velocity is zero. Such a vortex is not stable, because a velocity field can continuously change to zero everywhere.

In some special materials there can exist vector fields, associated to spin or other such property, that cannot vanish. Then it is possible to have vortices that are both non-singular and conserved, the conservation following from topological reasons. (One example is the continuous unlocked vortex (CUV) in superfluid ³He-A⁶.) The

prototype model that contains non-vanishing topological structures characterized by a Hopf charge was presented by L. Faddeev^{9,26}, and recently it has been shown numerically that this model does indeed contain stable topological solitons^{10,11,12,13}.

In this work we study numerically a system of two electromagnetically coupled, oppositely charged Bose condensates described by the Ginzburg-Landau (GL) model. Babaev *et al.* studied this system in Ref.²⁷ and argued that it should contain stable knotted vortex solitons with non-zero Hopf charge. Here we present our results for the GL model, the main conclusion being that Hopfions in the GL model are not stable, mainly due to leakage of topological charge into the electromagnetic field and the resulting instability against scaling.

The paper is organized as follows: In Section II we formulate the equations, discuss the possible potentials and present the initial states that are used in the computation. In Section III we present the discretization of the GL Lagrangian and the numerical method for finding stable minimum energy configurations. In Section IV we describe the results and finally in Section V we give some concluding remarks on the results obtained, including possible scenarios under which stability could be restored.

II. MODEL

A. Ginzburg-Landau model

The model describes two electromagnetically coupled, oppositely charged Bose condensates, as given by the GL

Lagrangian density

$$\mathcal{L} = \frac{\hbar^2}{2m_1} \left| (\nabla + i\frac{2e}{\hbar c} \vec{A}) \Psi_1 \right|^2 + \frac{\hbar^2}{2m_2} \left| (\nabla - i\frac{2e}{\hbar c} \vec{A}) \Psi_2 \right|^2 + V(\Psi_1, \Psi_2) + \frac{1}{2\mu_0} \vec{B}^2, \quad (1)$$

where we have used SI units. In Eq. (1) Ψ_1 and Ψ_2 are the order parameters for the condensates, \vec{A} is the electromagnetic vector potential, \vec{B} the magnetic field, $\vec{B} = \frac{1}{c} \nabla \times \vec{A}$, and V is a potential.

Babaev *et al.*²⁷ introduced new variables by setting

$$\Psi_\alpha = \sqrt{2m_\alpha \rho} \chi_\alpha, \quad (2)$$

where the new complex field χ is normalized as

$$|\chi_1|^2 + |\chi_2|^2 = 1, \quad (3)$$

and therefore the real field ρ is given by

$$\rho^2 = \frac{1}{2} \left(\frac{|\Psi_1|^2}{m_1} + \frac{|\Psi_2|^2}{m_2} \right). \quad (4)$$

In terms of the new fields of (2) Eq. (1) becomes

$$\mathcal{L} = \hbar^2 \rho^2 \left(\left| (\nabla + i\frac{2e}{\hbar c} \vec{A}) \chi_1 \right|^2 + \left| (\nabla - i\frac{2e}{\hbar c} \vec{A}) \chi_2 \right|^2 \right) + \hbar^2 (\nabla \rho)^2 + V(\chi_1, \chi_2, \rho^2) + \frac{1}{2\mu_0} \vec{B}^2. \quad (5)$$

The Lagrangian (1) is invariant under the gauge transformation

$$\begin{cases} \Psi_1 & \rightarrow e^{-i\frac{2e}{\hbar} \theta(x)} \Psi_1 \\ \Psi_2 & \rightarrow e^{i\frac{2e}{\hbar} \theta(x)} \Psi_2 \\ A_\mu & \rightarrow A_\mu + c \partial_\mu \theta(x), \end{cases} \quad (6)$$

and the corresponding Nöther current is

$$J_k = \frac{i\hbar e}{m_1} (\Psi_1^* \partial_k \Psi_1 - \Psi_1 \partial_k \Psi_1^*) - \frac{i\hbar e}{m_2} (\Psi_2^* \partial_k \Psi_2 - \Psi_2 \partial_k \Psi_2^*) - \frac{4e^2}{c} \left(\frac{|\Psi_1|^2}{m_1} + \frac{|\Psi_2|^2}{m_2} \right) A_k. \quad (7)$$

When we use the new variables (2) here, we obtain

$$\begin{aligned} J_k &= 2e\hbar\rho^2 i (\chi_1^* \partial_k \chi_1 - \chi_1 \partial_k \chi_1^* - \chi_2^* \partial_k \chi_2 + \chi_2 \partial_k \chi_2^*) \\ &\quad - \frac{8e^2 \rho^2}{c} A_k \\ &= 4e\hbar\rho^2 \left(\frac{1}{2} j_k - \frac{2e}{\hbar c} A_k \right), \end{aligned} \quad (8)$$

which contains a new (non-gauge invariant) current²⁸

$$j_k = i (\chi_1^* \partial_k \chi_1 - \chi_1 \partial_k \chi_1^* - \chi_2^* \partial_k \chi_2 + \chi_2 \partial_k \chi_2^*). \quad (9)$$

Later on we also use a gauge invariant vector field

$$\vec{C} = \frac{1}{\hbar e \rho^2} \vec{J}. \quad (10)$$

Next we define the unit vector field \vec{n} by

$$\vec{n} = (\chi_1^* \ \chi_2) \vec{\sigma} \begin{pmatrix} \chi_1 \\ \chi_2^* \end{pmatrix} = \begin{pmatrix} \chi_1 \chi_2 + \chi_1^* \chi_2^* \\ i(\chi_1 \chi_2 - \chi_1^* \chi_2^*) \\ |\chi_1|^2 - |\chi_2|^2 \end{pmatrix}, \quad (11)$$

where $\vec{\sigma}$ are the Pauli matrices. The inverse transformation is

$$\begin{cases} \chi_1 &= \frac{n_1 - i n_3}{\sqrt{2(1-n_3)}} e^{i\alpha}, \\ \chi_2 &= \frac{\sqrt{1-n_3}}{\sqrt{2}} e^{-i\alpha}, \end{cases} \quad (12)$$

where the phase α cannot be determined from \vec{n} .

The aim is now to write the Lagrangian (5) in terms of \vec{n} , ρ and \vec{C} , after which the \vec{n} part of the result should be similar to the FS model, given by

$$\mathcal{L}_{\text{FS}} = \frac{1}{2} \partial_k n_l \partial^k n^l + g_{\text{FS}} (\vec{n} \cdot \partial_k \vec{n} \times \partial_l \vec{n})^2. \quad (13)$$

After inverting Eqs. (8) and (10) to obtain \vec{A} in terms of \vec{C} and \vec{j} the kinetic part of Eq. (5) becomes

$$\mathcal{L}_{\text{kinetic}} = \hbar^2 \rho^2 (|\nabla \chi_1|^2 + |\nabla \chi_2|^2 - \frac{1}{4} \vec{j}^2) + \hbar^2 (\nabla \rho)^2 + \frac{\hbar^2 \rho^2}{16} \vec{C}^2. \quad (14)$$

Using Eqs. (11), (3) and (9) one finds that

$$\partial_k n_l \partial^k n^l = 4(|\nabla \chi_1|^2 + |\nabla \chi_2|^2) - \vec{j}^2 \quad (15)$$

and therefore the first term in Eq. (14) corresponds to the first term in Eq. (13).

By direct substitution of Eqs. (8) and (10) into \vec{B} , we also find that

$$\vec{B} = \frac{1}{c} \nabla \times \vec{A} = \frac{\hbar}{4e} (\nabla \times \vec{j} - \frac{1}{2} \nabla \times \vec{C}), \quad (16)$$

and again using Eqs. (11), (3) and (9), we get

$$\frac{1}{2} \epsilon_{klm} \vec{n} \cdot \partial_l \vec{n} \times \partial_m \vec{n} = -\epsilon_{klm} \partial_l j_m, \quad (17)$$

from which we can see that the \vec{B}^2 term in Eq. (5) contributes to the second term in Eq. (13).

Combining the above results we can write the Lagrangian (1) in the form

$$\mathcal{L} = \frac{\hbar^2 \rho^2}{4} \partial_k n_l \partial^k n^l + \hbar^2 (\nabla \rho)^2 + \frac{\hbar^2 \rho^2}{16} \vec{C}^2 + V(\rho, n_k) + \frac{\hbar^2}{128 \mu_0 e^2} [\epsilon_{klm} (\vec{n} \cdot \partial_k \vec{n} \times \partial_l \vec{n} + \partial_k C_l)]^2, \quad (18)$$

which is the form derived by Babaev *et al.*²⁷. The dynamical fields are now ρ , \vec{n} and \vec{C} . If $\rho = \text{constant}$ and $\vec{C} = 0$, the GL model reduces to the FS model in Eq. (13). Since the FS model contains stable topological structures with non-trivial Hopf charge, one can hope that the GL model also contains similar structures. However, GL contains the additional fields ρ and \vec{C} in comparison to FS and the role of these new fields must be investigated.

B. Form of the potential

A typical and rather general quartic potential used in the GL model is

$$V_0(\Psi_1, \Psi_2) = \frac{1}{2} c_1 |\Psi_1|^4 + \frac{1}{2} c_2 |\Psi_2|^4 + c_3 |\Psi_1|^2 |\Psi_2|^2 + b_1 |\Psi_1|^2 + b_2 |\Psi_2|^2 + a_0. \quad (19)$$

When Ψ 's are expressed in terms of ρ and \vec{n} and the whole system is rescaled so that $m_\alpha \rightarrow 1$, we find

$$|\Psi_1|^2 = \rho^2(1 + n_3), \quad |\Psi_2|^2 = \rho^2(1 - n_3), \quad (20)$$

and then the potential (19) reads

$$\begin{aligned} V_0(\rho^2, n_3) = & \rho^4 [n_3^2 (\frac{1}{2}(c_1 + c_2) - c_3) + n_3(c_1 - c_2) \\ & + \frac{1}{2}(c_1 + c_2) + c_3] \\ & + \rho^2 [n_3(b_1 - b_2) + b_1 + b_2] + a_0. \end{aligned} \quad (21)$$

One important aspect in choosing the potential is that at infinity the fields will settle to the minimum of the potential. Furthermore, in order to define the Hopf charge it is necessary that the \vec{n} field points to the same direction far away, otherwise we cannot compactify the 3D-space. It would therefore be optimal to have a potential with a minimum that would fix the \vec{n} field completely, say, to $n_3 = 1$. This may not happen for physically interesting potentials.

For a particular example assume that $c := c_1 = c_2 = c_3 > 0$, $b := b_1 = b_2$, then n_3 disappears from Eq. (21) and the potential minimum is at $\rho^2 = -b/(2c)$, \vec{n} being free. For more generic parameter values the extrema are obtained for particular values of n_3 and ρ^2 :

$$n_3 = \frac{b_1(c_2 + c_3) - b_2(c_1 + c_3)}{b_1(c_2 - c_3) + b_2(c_1 - c_3)}, \quad (22)$$

$$\rho^2 = -\frac{b_1(c_2 - c_3) + b_2(c_1 - c_3)}{2(c_1 c_2 - c_3^2)}. \quad (23)$$

This is a minimum, if $c_1 c_2 > c_3^2$. Note that the above values do not necessarily fall within the allowed values for ρ^2 and n_3 , (i.e., $\rho^2 > 0$ and $|n_3| \leq 1$), in which case the extrema are on the boundaries of the allowed values.

From physical arguments the following special case is relevant²⁹

$$V_1(\Psi_1, \Psi_2) = \lambda \left((|\Psi_1|^2 - 1)^2 + (|\Psi_2|^2 - 1)^2 \right), \quad (24)$$

it breaks $O(3)$ to $O(2)$ and corresponds to two independently conserved condensates. It has a minimum at $n_3 = 0$, $\rho^2 = 1$. Another physically relevant²⁹ potential is

$$\begin{aligned} V_2(\Psi_1, \Psi_2) = & \lambda \left((|\Psi_1|^2 - 1)^2 + (|\Psi_2|^2 - 1)^2 \right) \\ & + c |\Psi_1 \Psi_2^* - \Psi_2 \Psi_1^*| + a_0, \end{aligned} \quad (25)$$

which breaks $O(3)$ completely. This corresponds to multi-band superconductors with inter-band Josephson effect²⁹. In terms of \vec{n} this potential is given (using Eq. (12))

$$V_2 = \lambda \frac{1}{2} n_3^2 + c \text{Im}[(n_2 - i n_1) e^{i2\alpha}] + b_0. \quad (26)$$

The minimum of this potential is located at $\rho^2 = 1/2$, $n_3 = \sqrt{1 - c^2/\lambda^2}$, while the specific values of n_1 and n_2 also depend on α , which is related to the phase of Ψ .

From the point of view of Hopf-charge conservation the possibility of $\rho = 0$ is problematic, even if this happens locally, because then the field \vec{n} is not defined. However, it has been argued³⁰ that quantum effects ensure that $\rho \neq 0$ everywhere. In classical field theories, like the present one, such expected quantum effects can be included through effective potentials. Since the main purpose of this effective potential is to guarantee that $\rho \neq 0$, its exact form is not so important. One such potential, which we will use later, is

$$\begin{aligned} V_{\text{eff}}(\Psi_1, \Psi_2) = & \frac{1}{4} \lambda (|\Psi_1|^2 + |\Psi_2|^2 - \rho_0^2)^2 \\ & + 2\gamma (|\Psi_1|^2 + |\Psi_2|^2)^{-1} + a_0. \end{aligned} \quad (27)$$

The constants ρ_0 and a_0 are determined by requiring that the minimum of the potential is at $\rho^2 = 1$ with a value of 0, yielding $\rho_0^2 = 2 - \gamma/\lambda$ and $a_0 = -\gamma - \frac{\gamma^2}{4\lambda}$.

C. Initial states of Hopf invariant Q

We are interested in the minimum energy configurations of topologically distinct configurations of the vector field \vec{n} , related to the complex physical fields Ψ_α through Eqs. (2) and (12). From the point of view of \vec{n} it is only necessary that $\lim_{|\vec{x}| \rightarrow \infty} \vec{n} = \vec{n}_\infty$ is the same in all directions. From this it follows that we can compactify $\mathbb{R}^3 \rightarrow \mathbb{S}^3$ and then \vec{n} becomes a map $\mathbb{S}^3 \rightarrow \mathbb{S}^2$ with homotopy group $\pi_3(\mathbb{S}^2) = \mathbb{Z}$, characterized by the Hopf charge.

Therefore, we have to create a configuration with $\Psi_\alpha : \mathbb{R}^3 \rightarrow \mathbb{C}^2$ and $\vec{A} : \mathbb{R}^3 \rightarrow \mathbb{R}^3$, such that \vec{n} has the desired property mentioned above. For Ψ_α this implies $|\Psi_1|^2 + |\Psi_2|^2 \neq 0$ and $\lim_{|\vec{x}| \rightarrow \infty} \Psi_\alpha$ are (independent) constants. The first condition is also necessary for defining the field χ and if the second condition is also satisfied χ becomes a map $\mathbb{S}^3 \rightarrow \mathbb{S}^3$.

The method of constructing a configuration with a desired Hopf charge has been solved by Aratyn *et al.*³¹. The idea is to use the combination of any map $\phi : \mathbb{S}^3 \rightarrow \mathbb{S}^3$ with the Hopf map $h : \mathbb{S}^3 \rightarrow \mathbb{S}^2$

$$h(\phi_1, \phi_2, \phi_3, \phi_4) = \begin{pmatrix} 2(\phi_1 \phi_3 - \phi_2 \phi_4) \\ -2(\phi_1 \phi_4 + \phi_2 \phi_3) \\ \phi_1^2 + \phi_2^2 - \phi_3^2 - \phi_4^2 \end{pmatrix} \quad (28)$$

to give $h \circ \phi : \mathbb{S}^3 \rightarrow \mathbb{S}^2$.

For an explicit construction one uses the toroidal coordinates (η, ξ, φ) of \mathbb{R}^3 defined by

$$\begin{aligned} x_1 = \frac{\sinh(\eta) \cos(\varphi)}{q}, \quad x_2 = \frac{\sinh(\eta) \sin(\varphi)}{q}, \\ x_3 = \frac{\sin(\xi)}{q}, \quad q = \cosh(\eta) - \cos(\xi). \end{aligned} \quad (29)$$

Next take any monotonic function $g : [0, \infty) \rightarrow [-1, 1]$,

choose $p, q \in \mathbb{Z}$ and define the map $\phi: S^3 \rightarrow S^3$ by

$$\phi = (g(\eta) \cos(p\xi), g(\eta) \sin(p\xi), \sqrt{1-g(\eta)^2} \cos(q\varphi), \sqrt{1-g(\eta)^2} \sin(q\varphi)). \quad (30)$$

If furthermore g is such that $\lim_{\eta \rightarrow \infty} g^2(\eta) - \lim_{\eta \rightarrow 0} g^2(\eta) = 1$, then the combined map, $h \circ \phi$, has the Hopf invariant

$$H(h \circ \phi) = pq. \quad (31)$$

For details, see Ref.³¹.

Using Eqs. (11) and (30) and identifying

$$\phi_1 + i\phi_2 = \chi_1 \quad (32a)$$

$$\phi_3 + i\phi_4 = \chi_2, \quad (32b)$$

we obtain the following form for \vec{n}

$$\vec{n}(x) = \begin{pmatrix} 2g(\eta) \sqrt{1-g^2} \cos(p\xi + q\varphi) \\ -2g(\eta) \sqrt{1-g^2} \sin(p\xi + q\varphi) \\ 2g^2(\eta) - 1 \end{pmatrix}. \quad (33)$$

Note that the value of $\vec{n}_\infty := \lim_{|\vec{x}| \rightarrow \infty} \vec{n}$ (or, equivalently, $\Psi_\infty := \lim_{|\vec{x}| \rightarrow \infty} \Psi$) can be arbitrary, but in order to obtain a finite energy we must have $V(\Psi_\infty) = 0$. It is worth noting that fixing \vec{n} is not enough to determine the value of ρ^2 , but the choice of potential which dictates the value of $\lim_{|\vec{x}| \rightarrow \infty} \Psi_\alpha$ above, simultaneously fixes the *preferred* value of ρ^2 . We use this preferred value for all \vec{x} when constructing the initial configurations.

Inverting the toroidal coordinates defined in Eq. (29) enables us to express Eq. (30) in the cartesian coordinates. In addition, denoting $r^2 = x_1^2 + x_2^2 + x_3^2$ and using Eq. (32) in Eq. (2), we obtain

$$\Psi_1(x) = \frac{\left((r^2 - 1)^2 + 4x_3^2\right)^{\frac{1-p}{2}} (r^2 - 1 - 2ix_3)^p}{r^2 + 1} \quad (34a)$$

$$\Psi_2(x) = \frac{2\left(x_1^2 + x_2^2\right)^{\frac{1-q}{2}} (x_1 + ix_2)^q}{r^2 + 1}. \quad (34b)$$

This is the formula used for the initial configurations of Ψ_α for our numerical computations.

It is perhaps useful to mention once more that the change of variables in Eqs. (2)–(4) is not reversible whenever $\rho(\vec{x}) = 0$. There is, however, no guarantee that ρ stays non-zero in numerical simulations of the physical fields Ψ_α and \vec{A} , even if the minimum of the potential is at a non-zero value of ρ . The situation when $\rho = 0$ locally can imply breakdown in topology and therefore in our numerical simulations we have followed the changes in the global minimum value of ρ . It is also worth mentioning that, as we will see later, the discrete nature of a lattice simulation only approximates a continuous deformation and therefore it may occur that the approximation is not good enough, allowing a jump from one homotopy class to another.

III. NUMERICS

In this section we will describe the discretization of the model and the method of the minimization of the Lagrangian (1). We will also compare the GL to FS model and present some test calculations and the parameters as well as coupling constants for the simulations.

For simplicity we have used the rescaled $(|\Psi_\alpha|^2/m_\alpha \rightarrow |\Psi_\alpha|^2)$ Lagrangian and natural units ($c = \hbar = 1$) throughout our numerical work. With these choices, the Lagrangian density used in all our numerical simulations becomes

$$\mathcal{L} = \frac{1}{2} \left| (\nabla + ig\vec{A})\Psi_1 \right|^2 + \frac{1}{2} \left| (\nabla - ig\vec{A})\Psi_2 \right|^2 + \frac{1}{2} g_f (\nabla \times \vec{A})^2 + V_{1,\text{eff}}(\Psi_{1,2}). \quad (35)$$

This can be further scaled by $\vec{A} \rightarrow \frac{1}{g}\vec{A}$, which reveals the fact that the only relevant parameter is $g^2/g_f = 4\mu_0 e^2$. The values used in numerical simulations are $g = 1$ and $g_f = 2$, which amounts to a particular choice of units for μ_0 and e .

A. Discretization

The system has been discretized on a cubic rectangular lattice (indexed as (s, u, v)) with periodic boundary conditions. Our model can be considered as a two-component version of the time-independent, ordinary Abelian $U(1)$ Higgs model, which has long since been discretized for lattice simulations in quantum field theory (for example, see Ref.^{32,33} and references therein). The main point in that context is to discretize the fields so that gauge invariance is preserved. From Eq. (6) we see that if we use the forward discretization of the derivatives, the gauge transformation of A_k has to be discretized as follows:

$$A_{1|s,u,v} \rightarrow A_{1|s,u,v} + \frac{c}{a} (\theta_{s+1,u,v} - \theta_{s,u,v}), \quad (36a)$$

$$A_{2|s,u,v} \rightarrow A_{2|s,u,v} + \frac{c}{a} (\theta_{s,u+1,v} - \theta_{s,u,v}), \quad (36b)$$

$$A_{3|s,u,v} \rightarrow A_{3|s,u,v} + \frac{c}{a} (\theta_{s,u,v+1} - \theta_{s,u,v}), \quad (36c)$$

where a is the lattice parameter. Thus, A_k should be considered as living on the link between two lattice points parallel to the coordinate axis k . Combining this discretization with the way the Ψ_α transforms in Eq. (6) it follows that the following combination

$$\begin{aligned} & \Psi_{1|s+1,u,v}^* \Psi_{1|s,u,v} e^{-ia\kappa A_{1|s,u,v}} \\ & + \Psi_{1|s+1,u,v} \Psi_{1|s,u,v}^* e^{ia\kappa A_{1|s,u,v}} \\ & - \Psi_{1|s+1,u,v}^* \Psi_{1|s+1,u,v} - \Psi_{1|s,u,v}^* \Psi_{1|s,u,v}, \end{aligned} \quad (37)$$

where $\kappa = \frac{2e}{\hbar c}$, is gauge invariant. If we calculate its continuum limit as $a \rightarrow 0$ by expanding in a (e.g., $\Psi_{1|s+1,u,v} = \Psi_1(x + a, y, z) = \Psi_1(x, y, z) + a\partial_x \Psi_1(x, y, z) + \frac{1}{2}a^2\partial_x^2 \Psi_1(x, y, z) + \dots$) we

obtain $-a^2|(\partial_1 + i\kappa A_1)\Psi_1|^2 + O(a^3)$. For Ψ_2 with A_1 we use a similar expression with $\kappa \rightarrow -\kappa$. Finally, for the other components of \vec{A} we use corresponding shifts, as illustrated in Eqs. (36) and (37).

For the discretization of \vec{B}^2 we use the expression

$$e^{iF_{12|su v}} + e^{-iF_{12|su v}} + e^{iF_{23|su v}} + e^{-iF_{23|su v}} + e^{iF_{31|su v}} + e^{-iF_{31|su v}} - 6, \quad (38)$$

where, for example,

$$F_{12|su v} = A_{1,s,u+1,v} - A_{1,s,u,v} - A_{2,s+1,u,v} + A_{2,s,u,v}. \quad (39)$$

The F_{kl} are gauge invariant under Eq. (36), and the continuum limit of Eq. (38) with Eq. (39) is $-a^2(\nabla \times \vec{A})^2 + O(a^3)$.

For the potential we use $a^2 V(\Psi_{\alpha|su v})$. The discretized Lagrangian is the sum of all the above terms multiplied by $-a/2$, and then the resulting sum has the continuum limit of Eq. (35). In practice we use the cubic grids of sizes of $120^3 \dots 960^3$. Of these just the sizes 240^3 , 480^3 and 720^3 are used in actual simulations, the remaining sizes used only to verify the code, results and discretization.

The minimization of the Lagrangian has been done using the steepest descent method. The gradients needed have been calculated symbolically from the discretized Lagrangian.

B. Initial states

In order to start the simulations we have to generate initial states with specified Hopf invariants. These initial configurations have been made using Eq. (34) and choosing ρ such that $V(\Psi_\infty) = 0$. However, this leaves \vec{A} undetermined. The topology of the system is unaffected by \vec{A} , so in principle, we can choose any configuration for it. We have used several different initial configurations for \vec{A} ; most commonly the one defined by the condition $\vec{C} = 0 \Rightarrow \vec{A} = \frac{\hbar c}{4e} \vec{j}$, by Eqs. (9) and (10). This choice enables us to test the validity of the program by comparing the energies of the initial states with those obtained for the pure FS model. As a further test of discretization we used the same initial configuration in grids of different sizes and with different lattice constants. With grid sizes of 240^3 and above the energies were within 1% of each other.

C. Comparison with previous FS studies

We have also compared the new calculations with those presented in Ref.¹³. By using an initial configuration, where $\rho \equiv 1$, $\vec{C} \equiv 0$ and $V \equiv 0$, the GL model (18) reduces to the FS model (13). In particular, the magnetic

term becomes $E_{MB} = \frac{\hbar^2}{128\mu_0 e^2} [\epsilon_{klm} (\vec{n} \cdot \partial_l \vec{n} \times \partial_m \vec{n})]^2$, while in the FS model we have $E_{TFS} = \frac{1}{2} g_{FS} (\vec{n} \cdot \partial_k \vec{n} \times \partial_l \vec{n})^2$. If we set $c = \hbar = 1$, $e = \frac{1}{2}$, $\mu_0 = 1$ and $g_{FS} = \frac{1}{8}$ (the value most commonly used in our earlier work), we have $E_{TFS} = 2E_{MB}$. We created the same initial configuration with our old and new codes and found that the energies of the initial states agree to within 1 % with a grid of 120^3 .

In our previous studies we have always assumed that $\lim_{|x| \rightarrow \infty} n_3 = 1$, but some of the present potentials, e.g., V_1 , do not have that as a minimum. In this case we may assume that $\lim_{|x| \rightarrow \infty} n_2 = 1$, but this can be transformed to $n_3 = 1$ by a global rotation in the configuration space, which takes $n_3 \rightarrow n_2$ and $n_2 \rightarrow -n_3$. The same effect can be achieved by using new fields defined by

$$\Psi'_1 = \frac{1}{\sqrt{2}}(\Psi_1 + i\Psi_2^*), \quad \Psi'_2 = \frac{1}{\sqrt{2}}(\Psi_2 - i\Psi_1^*). \quad (40)$$

During the calculations we have monitored the topology of the system. As we saw in Sec. II B, the conservation of topology is not guaranteed whenever $\rho \rightarrow 0$. Therefore we have followed the value of the global minimum of ρ^2 . In keeping with our earlier work, we have also monitored the dot products of $\vec{n}(\vec{x}) \cdot \vec{n}(\vec{x} + \vec{\mu})$, (where $\vec{\mu} \in \{(1, 0, 0), (0, 1, 0), (0, 0, 1)\}$). When the global minimum of this dot product approaches zero or becomes even negative it indicates possible breakdown of topology during the simulation.

We have also calculated the value of Hopf invariant directly from the field configuration. Using the basic differential geometric result of $H(h \circ \chi \equiv \vec{n}) = \deg \chi$, we can even use our computational field variables. Since for any map $f \in C^\infty(S^3, S^3)$,

$$\deg f = \frac{1}{2 \cdot 3! \pi^2} \int_{S^3} \epsilon_{\mu\nu\sigma\rho} f^\mu df^\nu \wedge df^\sigma \wedge df^\rho, \quad (41)$$

we can compute the value of the Hopf invariant by numerical integration. The Hopf invariant can also be determined by visual inspection of linking numbers of pre-images.

IV. RESULTS AND DISCUSSION

A. Stability of topological structures

A necessary condition for any stable static localized structure is its stability against scaling. Let us assume, for now, that $\rho \neq 0$ everywhere. The simple procedure of Derrick³⁴ then provides us with a necessary condition for the stability against scaling. Consider the behavior of the energy under scaling $x \rightarrow \lambda x$. For the FS model in 3D the volume element behaves like λ^3 while in the integrand (13) the first term scales as λ^{-2} and the second one as λ^{-4} . In the energy integral the two terms then have opposite behavior and if each is positive definite, one cannot scale the energy to zero. Indeed, one can

show³⁵ that in the FS model the energy is bounded from below by the Hopf charge: $E > c|Q|^{3/4}$. This has also been confirmed numerically^{10,11,12,13}.

In the present model the stability hinges on the behavior of the first and last terms in Eq. (18). The scaling properties of these two terms are opposite and thus, as long as they are both non-zero, the system is stable. The last term, however, equals the term \vec{B}^2 in Eq. (1) and could, in principle, vanish. Indeed, if the \vec{C} field obtains the value

$$\epsilon_{klm}\partial_l C_m = -\epsilon_{klm}\vec{n} \cdot \partial_l \vec{n} \times \partial_m \vec{n}, \quad (42)$$

then the last term vanishes and the system is no longer stable under scaling. Equation (42) can be satisfied, since \vec{C} contains \vec{A} , which is in principle free.

Another possibility for topology breakdown is if ρ vanishes, even locally. This means $\Psi_\alpha = 0$ and we have no longer either of the superconducting phases but instead a normal phase. It also follows that both χ_α and \vec{n} are then undetermined. From the point of view of \vec{n} this means that suddenly its domain is no longer the full S^3 , but rather S^3 with some points removed. The arguments about topological charge no longer hold and topology can break. This opens up the possibility of \vec{n} to change discontinuously in the domain where $\rho = 0$.

B. Numerical simulations

We have investigated the two component GL model using un-knot initial states with non-vanishing topological charge $Q = H(\vec{n})$. The computational parameters of the system are shown in Table I.

$H(\vec{n})$	p	q	N	a
1	1	1	120, 240, 480, 720, 960	$10.0/N$
2	1	2	240, 480, 720, 960	$10.0/N$
2	2	1	240, 480	$10.0/N$
3	1	3	240	$10.0/N$
4	2	2	240	$9.0/N$

TABLE I: Initial configurations. Hopf invariant $H(\vec{n}) = \deg \Phi$, constants p and q from Eq. (30), number of grid points per axis N , and the lattice constant a .

In all simulations of Table I, with potentials V_0 , V_1 and V_{eff} , the overall behavior is the same. As the iterations proceed the value of the field ρ^2 drops down to 0 locally while at the same time the dot product $\vec{n}(\vec{x}) \cdot \vec{n}(\vec{x} + \vec{\mu})$ goes to -1 , see Fig. 1. (Since we use Ψ_α in the computation and not \vec{n} , the dot product is computed by writing it as a function of Ψ_α with the help of Eqs. (2), (3), and (11).) The fact that two neighboring \vec{n} -vectors are anti-parallel implies that some part of the vortex configuration has shrunk to a size less than the lattice constant. We have also verified that the events, $\rho = 0$ and $\vec{n}(\vec{x}) \cdot \vec{n}(\vec{x} + \vec{\mu}) = -1$, occur at the same location.

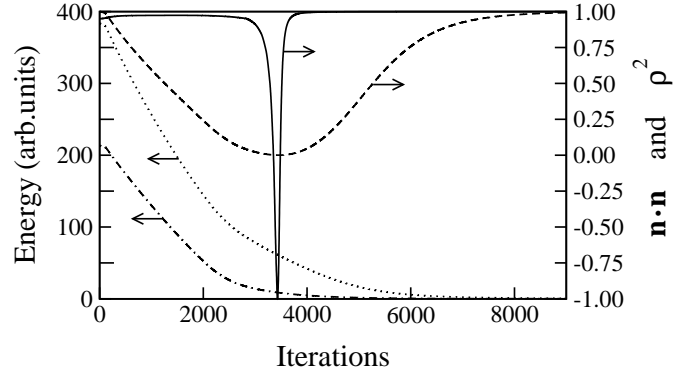


FIG. 1: Total energy (dotted line), energy of the \vec{B}^2 term (dash-dotted line), the global minimum of the deviations of nearest-neighbor \vec{n} vectors in the lattice (solid line) ($\vec{n} \cdot \vec{n} = 1$ indicates parallel and $\vec{n} \cdot \vec{n} = -1$ anti-parallel orientation), and the global minimum of ρ^2 (dashed line) as a function of the number of iterations during the relaxation of the $(p, q) = (1, 2)$ un-knot.

The topology breakdown can also be determined visually. The illustration in Fig. 2 shows the pre-image of some latitude circle, that is, the surface where the vector field \vec{n} has a fixed angle with the vacuum direction, i.e., where n_3 has a fixed value. The longitude is described by colors (gray-scale) on the iso-latitude surface. This is suitable because colors are commonly put on a circle anyway: magenta \rightarrow yellow \rightarrow green \rightarrow cyan \rightarrow magenta. (The actual position of the zero meridian is not important, because it is a gauge dependent quantity.) Two points, $n_1 = 1$ and $n_2 = 1$, have been chosen from the latitude circle and their pre-images are illustrated by the red (dark gray) and blue (black) tubes along the iso-surface. The linking number of these pre-images can be used to find the Hopf invariant of the system and it is clearly seen to go from 2 to 0 in the image sequence.

The behavior described above agrees with the scenarios discussed in the previous subsection: The quantity ρ^2 going to zero indicates that a small volume of non-superconducting phase has formed in the system, and also that Eq. (11) is not well defined as discussed in Sec. II C. During the process where $\rho^2 \rightarrow 0$ it also occurs that the energy of the B^2 term in the Lagrangian approaches zero (see Fig. 1). As mentioned above, this allows scaling and indeed both the radii of the torus decrease to zero (the smaller radius is defined by the iso-surface of some specific value of n_3 , say $n_3 = 0$). For each system the total energy also decreases to zero monotonously.

We have also investigated whether the strength of the potential, i.e., the value of λ in Eq. (24), changes the behavior of the system. It turns out that the parameter λ only has an effect on the speed with which the minimum energy configuration is found: The stronger the potential, the slower the process, but nevertheless the topology always breaks down. Furthermore, increasing the number of lattice points cannot prevent the topology from

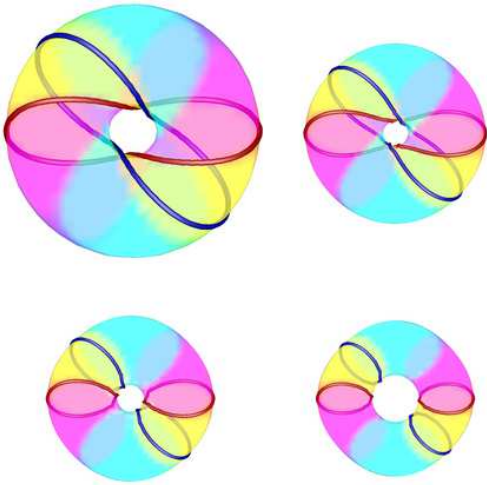


FIG. 2: Snapshots of the pre-images in the relaxation of the $(p, q) = (1, 2)$ un-knot, after 0 (top left), 3300 (top right), 3500 (down left), and 3600 (down right) iterations. Topology breaks between iterations 3300 and 3500.

breaking down either, because the scaling can go all the way to zero when $\vec{B}^2 = 0$. (This is in contrast with the FS model, where we sometimes had tightly knotted configurations whose structure was eventually resolved by increasing the lattice density.)

In the above the topology breakdown was associated with $\rho \rightarrow 0$ locally. What if this is prevented by quantum effects, or in our classical field theory, by an effective potential V_{eff} in Eq. (27), or by keeping the value of ρ^2 fixed to a constant non-zero value? Simulations for an un-knot, i.e., torus of a charge $Q = 1$ in a lattice of 240^3 using the effective potential V_{eff} show that the global minimum of ρ^2 decreases from its initial value as before, but now it drops down to a non-zero value after which it starts to increase again. Simultaneously the dot product $\vec{n}(\vec{x}) \cdot \vec{n}(\vec{x} + \vec{\mu})$, nevertheless, goes to -1 locally. Increasing the lattice density to 480^3 or 720^3 grid points does not change the qualitative behavior of the system. The global minimum of ρ^2 goes to a lower but still non-zero value and there are still anti-parallel nearest-neighbor \vec{n} vectors in some region of the system. Even keeping the value of ρ^2 fixed to a constant non-zero value does not change this behavior.

In all cases the topology of the systems eventually breaks down by the same scenario: First, topological charge leaks from \vec{n} to \vec{C} , so that $\vec{B} \rightarrow 0$. This holds irrespective of the initial state of \vec{A} . After this the system can scale so that the region that contributes to the topological charge becomes smaller and smaller, eventually falling into the space between the lattice points. The form of the potential does not change this, because it does not change the scaling properties of the system.

The fact that the torus is transformed to a singular

line can also be seen by monitoring the Hopf invariant in the system using Eq. (41) in the numerical integrations: The denser the grid, the sharper the drop of the charge from the original value to zero. We also checked this by plotting the Hopf invariant density (i.e. the value of the integrand in Eq. (41)) for some of these systems and found it to concentrate ever more tightly around the vortex core. This tells us that the region contributing to the charge will eventually be in between the grid points used in the computation. Thus, it is not possible to prevent the breakdown of the topology making the grid even denser.

It has to be noted that although the change of topology in its final stages is a consequence of the discreteness of the lattice, its fundamental cause, the fact that B^2 goes to zero which leads to scaling instability, is not. Thus, in a fully continuous analysis the conclusions would be the same.

V. CONCLUSIONS

We have investigated numerically the two-component Ginzburg-Landau model using torus un-knots, with non-vanishing Hopf charge Q , as initial states; this brings a topological structure into the system. We have used different types of potentials depending on both of the order parameters Ψ_α of the system. In all the cases the system behaves similarly, i.e., the topological structure of the system eventually disappears, contrary to the case of the Faddeev-Skyrme model. The topological stability in the FS model is due to the fact that the kinetic and topological terms are non-vanishing and have an opposite behavior in the scaling. In the GL model, the term corresponding to the FS topological term is the magnetic field term which, however, can vanish, after which the system becomes unstable against scaling. This is indeed what happens during energy minimization.

Thus, it seems that the two-component GL model does not support stable topological structures having a non-trivial conserved Hopf invariant, due to this scaling instability. How could this breakdown of topology be prevented? There are a couple of possible scenarios to stabilize the system. One could try to somehow prevent the leakage of \vec{n} into \vec{C} , and therefore the vanishing of the B^2 term, which leads to scaling instability. This could be done by introducing terms that scale as (∂_k^d) with $d > 3$ or terms that make the system avoid states with $\vec{C} = 0$, as is done in Ref.³⁶. Both of these are, however, outside the scope of this article, since a model with such terms would describe vastly different physical systems than the ones considered here. Another possibility is that the Hopfions are in fact meta-stable or dynamically stable. This could happen if potential is very strong and the coupling constant g_f/g^2 very small. Still another possibility is to envelop the system in an external magnetic field, which would prevent the situation $\vec{B} \rightarrow 0$ at least on the boundaries of the system (up to London penetration depth).

These are all possibilities that merit further study.

Acknowledgments

We greatly acknowledge generous computing resources from the M-grid project, supported by the Academy of

Finland, and from CSC – Scientific Computing Ltd., Espoo, Finland. This work has partly been supported by the Academy of Finland through its Center of Excellence program. One of us (J.J.) also wishes to thank Jenny and Antti Wihuri Foundation for a supporting grant.

-
- * Electronic address: juolja@utu.fi
 - † Electronic address: hietarin@utu.fi
 - ‡ Electronic address: pts@fyslab.hut.fi
 - ¹ J. R. Abo-Shaer, C. Raman, J. M. Vogels, and W. Ketterle, *Science* **292**, 476 (2001).
 - ² P. Engels, I. Coddington, P. C. Haljan, V. Schweikhard, and E. A. Cornell, *Phys. Rev. Lett.* **90**, 170405 (2003).
 - ³ R. Monaco, J. Mygind, M. Aaroe, R. J. Rivers, and V. P. Koshelets (2005), cond-mat/0503707.
 - ⁴ R. Monaco, J. Mygind, and R. J. Rivers, *Phys. Rev. Lett.* **89**, 080603 (2002).
 - ⁵ R. Carmi, E. Polturak, and G. Koren, *Phys. Rev. Lett.* **84**, 4966 (2000).
 - ⁶ Ü. Parts, J. M. Karimäki, J. H. Koivuniemi, M. Krusius, V. M. H. Ruutu, E. V. Thuneberg, and G. E. Volovik, *Phys. Rev. Lett.* **75**, 3320 (1995).
 - ⁷ A. P. Finne, S. Boldarev, V. B. Eltsov, and M. Krusius, *Journal of Low Temperature Physics* **136**, 249 (2004).
 - ⁸ R. Ray and A. M. Srivastava, *Phys. Rev.* **D69**, 103525 (2004), hep-ph/0110165.
 - ⁹ L. D. Faddeev and A. J. Niemi, *Nature* **387**, 58 (1997), hep-th/9610193.
 - ¹⁰ R. A. Battye and P. M. Sutcliffe, *Phys. Rev. Lett.* **81**, 4798 (1998), hep-th/9808129.
 - ¹¹ R. A. Battye and P. Sutcliffe, *Proc. Roy. Soc. Lond.* **A455**, 4305 (1999), hep-th/9811077.
 - ¹² J. Hietarinta and P. Salo, *Phys. Lett.* **B451**, 60 (1999), hep-th/9811053.
 - ¹³ J. Hietarinta and P. Salo, *Phys. Rev.* **D62**, 081701(R) (2000).
 - ¹⁴ J. Hietarinta, J. Jäykkä, and P. Salo, *Phys. Lett.* **A321**, 324 (2004), cond-mat/0309499.
 - ¹⁵ C. Adam, J. Sanchez-Guillen, and A. Wereszczynski (2006), hep-th/0602008.
 - ¹⁶ J. P. Martikainen, A. Collin, and K. A. Suominen, *Phys. Rev. Lett.* **88**, 090404 (2002).
 - ¹⁷ M. Mackie, O. Dannenberg, J. Piilo, K.-A. Suominen, and J. Javanainen, *Phys. Rev.* **A69**, 053614 (2004), physics/0305057.
 - ¹⁸ J. Ruostekoski and Z. Dutton, *Phys. Rev.* **A72**, 063626 (2005), cond-mat/0507032.
 - ¹⁹ X.-J. Liu, H. Jing, X. Liu, and M.-L. Ge, *Eur. Phys. J. D* **37**, 261 (2006).
 - ²⁰ E. Smorgrav, J. Smiseth, E. Babaev, and A. Sudbo, *Phys. Rev. Lett.* **94**, 096401 (2005), cond-mat/0411031.
 - ²¹ M. Donaire, T. W. B. Kibble, and A. Rajantie (2004), cond-mat/0409172.
 - ²² V. B. Eltsov, A. P. Finne, R. Hanninen, J. Kopu, M. Krusius, M. Tsubota, and E. V. Thuneberg, *Phys. Rev. Lett.* **96**, 215302 (2006).
 - ²³ A. P. Finne, T. Araki, R. Blaauwgeers, V. B. Eltsov, N. B. Kopnin, M. Krusius, L. Skrbek, M. Tsubota, and G. E. Volovik, *Nature* **424**, 1022 (2003).
 - ²⁴ E. Babaev, A. Sudbo, and N. W. Ashcroft, *Nature* **431**, 666 (2004), cond-mat/0410408.
 - ²⁵ E. Babaev, *Phys. Rev.* **D70**, 043001 (2004), astro-ph/0211345.
 - ²⁶ L. D. Faddeev, *Letters in Mathematical Physics* **1**, 289 (1976).
 - ²⁷ E. Babaev, L. D. Faddeev, and A. J. Niemi, *Phys. Rev.* **B65**, 100512(R) (2002), cond-mat/0106152.
 - ²⁸ There seems to be contradiction in the sign of j_k between what we obtain here and what is obtained after Eq. (4) in Ref.²⁷. This affects some signs of other formulas as well.
 - ²⁹ E. Babaev, private communication.
 - ³⁰ L. Faddeev and A. J. Niemi, *Phys. Rev. Lett.* **85**, 3416 (2000), physics/0003083.
 - ³¹ H. Aratyn, L. A. Ferreira, and A. H. Zimerman, *Phys. Rev. Lett.* **83**, 1723 (1999), hep-th/9905079.
 - ³² K. G. Wilson, *Phys. Rev.* **D10**, 2445 (1974).
 - ³³ P. H. Damgaard and U. M. Heller, *Phys. Rev. Lett.* **60**, 1246 (1988).
 - ³⁴ G. H. Derrick, *J. Math. Phys.* **5**, 1252 (1964).
 - ³⁵ A. F. Vakulenko and L. V. Kapitanskii, *Sov.Phys.Dokl.* **24**, 433 (1979).
 - ³⁶ R. S. Ward, *Phys. Rev.* **D66**, 041701(R) (2002), hep-th/0207100.